Transition to Spatiotemporal Intermittency and Defect Turbulence in Systems under Translational Coupling

F. Alvarez-Garrido, M. G. Clerc, and G. Gonzalez-Cortes
Departamento de Física and Millennium Institute for Research in Optics, Facultad de Ciencias Físicas y Matemáticas, Universidad de Chile, Casilla 487-3, Santiago, Chile

(Received 4 November 2019; accepted 30 March 2020; published 21 April 2020)

Out of equilibrium systems under the influence of enough energy injection exhibit complex spatiotemporal behaviors. Based on a liquid crystal light valve experiment with translational optical feedback, we observe propagation, spatiotemporal intermittency, and defect turbulence of striped waves. A prototype model of pattern formation with translational coupling shows the same phenomenology. Close to the spatial instability, a local amplitude equation is derived. This amplitude equation allows us to reveal the origin and bifurcation diagram of the observed complex spatiotemporal dynamics. Experimental observations have a qualitative agreement with theoretical findings.

DOI: 10.1103/PhysRevLett.124.164101

Nonequilibrium processes often lead to the formation of dissipative structures in nature [1–4]. These processes are characterized by constantly injecting and dissipating energy. When the injection of energy is small compared to dissipation, equilibria are usually characterized by being uniform and stationary. Increasing the energy injection can develop a pattern from a homogeneous state through spontaneous breaking of symmetries [1–4]. At the onset of this instability, a general strategy to describe the dynamics is achieved through amplitude equations [3–5]. This description permits us to explain the emergence of stripes, hexagons, rhombic, quasicrystals, superlattice textures, and the alternation between them among other phenomena [3–7]. In nonlinear optics, the coupling of light to a polarizable medium is the primary mechanism of pattern formation (see review [8] and references therein). One of the difficulties to face is the proper alignment of the light since a small deviation can generate deformations and dynamics of patterns. This misalignment can trigger a transition from hexagon to stripe or square pattern [9,10]. From a theoretical point of view, optical misalignment can be modeled by *translational couplings*. Namely, the dynamics that are steering the system under study depend on physical variables in its local position and on what happens in a position at a given distance [10–12]. This type of dynamics can induce that localized patterns to propagate and even emit vortices with a structure such as von Kármán street [12]. Asymmetric differential integral terms can be described by translational couplings. This type of coupling has been used to describe the dynamical behaviors of several systems such as neurons [13], vegetation self-organization in nonuniform topography [14], fluid surface dynamics, and optical fibers [15]. Selection and transition of stationary two-dimensional patterns in optical experiments with translational coupling have been established [9,10]. However, the understanding of complex spatiotemporal patterns remains unexplored.

This Letter aims to investigate how the translational coupling in pattern-forming systems brings out the emergence and transition of complex spatiotemporal behaviors. Based on a liquid crystal light valve experiment with translational optical feedback, we observe the emergence of striped patterns. Increasing the length of the translational coupling, the system exhibits transitions to traveling, spatiotemporal intermittency, and defect turbulence of striped waves. A universal pattern model, the Turing-Swift-Hohenberg equation [16,17] with translational coupling, is analyzed. Increasing the length of the translational coupling, this model exhibits a transition between traveling, spatiotemporal intermittency, and defect turbulence of waves. Close to spatial instability, the complex Ginzburg-Landau equation is derived. This local model allows us to reveal the origin and bifurcation diagram of the observed dynamical behaviors. The sequence of experimental bifurcations and observations have a qualitative agreement with theoretical findings.

A flexible and straightforward experiment that displays pattern formation is the liquid crystal light valve (LCLV) with optical feedback (see review [18] and references therein). Figure 1 shows a schematic representation of a LCLV with an optical feedback. The LCLV is composed of a nematic liquid crystal (LC) film between a glass and a photoconductive plate. A dielectric mirror is deposed over the photoconductive plate. The LC film is planarly aligned, with a thickness $d = 15\ \mu$m. The liquid crystal used is a nematic LC-654 (NIOPIK) with positive dielectric anisotropy $\Delta\varepsilon = 10.7$, and large optical birefringence $\Delta n = 0.2$. To obtain the maximum polarization change on the light, we set an angle $\pi/4$ between the electric field orientation of the incident light and the anchoring of the

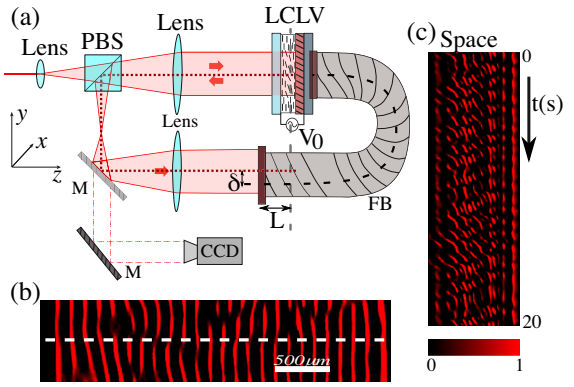

FIG. 1. (a) Schematic representation of the setup. LCLV is a liquid crystal light valve, PBS polarized beam splitter, M accounts for mirrors, V_0 the voltage applied to the liquid crystal layer, CCD charge-coupled device camera, L free propagation length, FB optical fiber bundle, and δ translational length. (b) Snapshot of the striped pattern obtained with $L = -4.0$ cm and $\delta = 50$ μm. (c) Spatiotemporal evolution of the profile of the striped pattern in the dashed line illustrated in (b).

cell. Transparent electrodes permit the application of an external electrical potential $V = V_0 \cos(\omega t)$ across the LC layer ($\omega = 1.0$ kHz). The LCLV is illuminated by an expanded He-Ne laser beam, $\lambda = 633$ nm, with 1.5 cm transverse radius and power $I_{\text{in}} = 7.0$ mW/cm^2. Once the light is injected into the LCLV, the beam is reflected by the dielectric mirror. Light is sent to the polarizing beam splitter cube (PBS), which will carry the light into the feedback loop given the polarization change the light has undergone in the LCLV. A nonpolarized beam splitter M and an optical fiber bundle (FB) have been used to close the loop. To record the liquid crystal cell plane, we collect the light with a coupled charge device (CCD) camera.

A $4-f$ array is placed in the optical feedback loop to obtain a self-imaging and the Fourier plane. By means of the optical fiber bundle, it is possible to adjust the free propagation length characterized by the L parameter [18]. In order to introduce a translational coupling on the LCLV, the FB also is displaced in a distance δ in the y direction (cf. Fig. 1) [9]. When considering a negative free propagation length and a translational coupling ($\delta \neq 0$), the hexagonal patterns become striped patterns. Figure 1(b) shows a typical striped pattern as the consequence of translational coupling. Unexpectedly, these patterns are not static. To characterize its dynamics, we monitor the spatiotemporal evolution of an arbitrary horizontal line of these patterns. Figure 1(c) illustrates the spatiotemporal dynamics exhibited by the LCLV with translational coupling. This dynamic behavior presents complex spatiotemporal evolution similar to that exhibited by the optical valve with an anisotropic filter in the Fourier plane [19]. Observe that if one considers another line, the dynamical behavior exhibited by the system is similar.

To shed light on the observed dynamics in the LCLV with optical feedback and translational coupling, let us consider a simplified mathematical model of pattern formation with translational coupling, which reads (the Swift-Hohenberg model with translational coupling [11])

$$\partial_t u(y,t) = \epsilon\tilde{u} - \tilde{u}^3 - \nu\partial_{yy}u - \partial_{yyyy}u, \tag{1}$$

where $u(y,t)$ is a scalar order parameter, y and t account for the spatial coordinate and time, respectively, $\tilde{u} \equiv u(y+\delta,t)$ stands for the translational coupling, ϵ is a bifurcation parameter, and ν accounts for the local spatial coupling (coupling to nearest neighbors). When ν is negative (positive) the term proportional to it accounts for a diffusive (antidiffusive) process. ∂_{yy} and ∂_{yyyy} are the Laplacian and bi-Laplacian operator, respectively. For the sake of simplicity, we consider periodic boundary conditions. A qualitatively similar model to Eq. (1) has been used to describe the LCLV with translational coupling [9]. When $\delta = 0$, model Eq. (1) becomes the Swift-Hohenberg model [20]. This paradigmatic equation was deduced originally to describe the pattern formation on Rayleigh-Bénard convection [20]. The Swift-Hohenberg equation is the most simple isotropic and reflection symmetry real model that shows pattern formation [4].

For $\epsilon < -\nu^2/4$ and $\delta = 0$, the only equilibrium presented by the model Eq. (1) is $u(y,t) = 0$. When $\epsilon \geq -\nu^2/4$ and $\delta = 0$, the model presents a family of motionless patterns of wave number of the order $\sqrt{\nu}$, which emerge through a supercritical transition. Figure 2(a) shows the spatiotemporal evolution and envelope of $u(y,t)$ of the typically observed pattern. The envelope of $u(y,t)$ is computed by the transformation $\mathcal{H}(y,t) = |\int_{-\infty}^{\infty}[\int_0^{\infty} u(y',t)e^{ik(y'-y)}dy']dk/\pi|$ [21]. In addition, the right panels display the temporal average of the power spectrum of the envelope $S(k) = \int_0^T |\int_{-\infty}^{\infty} \mathcal{H}(y,t)e^{-iky}dy|^2 dt/\sqrt{2\pi T}$. From this figure, we infer that the pattern has a well-defined dominant wavelength. By increasing the translational parameter, stationary patterns become propagative waves in a direction determined by the δ sign [see Fig. 2(b)]. Note that these waves are slightly asymmetric and have a uniform envelope. This propagative phenomenon can be understood as a result that small translational coupling induces linear and nonlinear drag effects [22]. Namely, it is possible to approximate the nonlocal term by $\tilde{u} \approx u(y,t) + \delta\partial_y u$ when $\delta \ll 1$.

Notwithstanding, when δ is large enough, uniform traveling waves suffer an instability that gives rise to the emergence of defects in the traveling wave. Defects are characterized by being zero of the envelope wave, i.e., the wave exhibits a phase singularity. Observe that defects separate regions with almost uniform wave amplitudes. Defect dynamics present complex spatiotemporal evolution characterized by generating triangular shaped regions of uniform wave amplitude with different sizes. Figure 2(c)

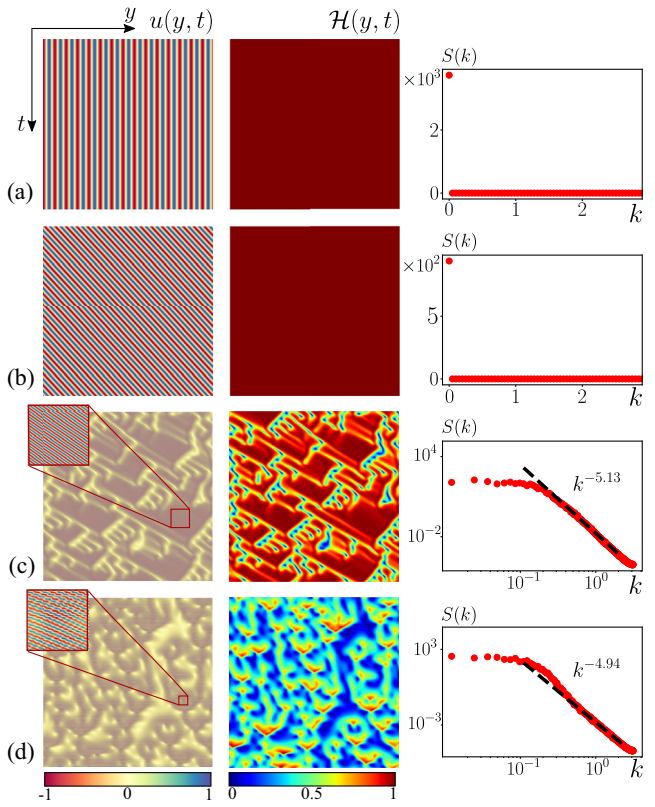

FIG. 2. Spatiotemporal evolution of patterns in the Swift-Hohenberg model with translational coupling Eq. (1). The left, center, and right panels are spatiotemporal diagrams of $u(y,t)$, envelope of $u(y,t)$ [$\mathcal{H}(u)$], and the temporal average power spectra $S(k)$ of the envelope. (a) $\epsilon = -0.08$, $\delta = 0.0$, (b) $\epsilon = -0.3$, $\delta = 1.0$, (c) $\epsilon = -0.3$, $\delta = 1.35$, and (d) $\epsilon = -0.8$, $\delta = 1.51$. The insets illustrate a magnification of the temporal space diagram.

shows the typical observed dynamics. The envelope $\mathcal{H}(y,t)$ allows us to clearly visualize the complex dynamics. Hence, in the spatiotemporal diagram, the system is characterized by presenting an alternation between regular and irregular region. This type of dynamical behavior is usually called spatiotemporal intermittency [23]. The temporal average of the power spectrum of the envelope allows us to find relationships between the dynamics of different spatial modes. Right panel of Fig. 2(c) illustrates this power spectrum $S(k)$. This spectrum is characterized by having a power law for large wave numbers, $S(k) \sim k^{-5}$. From this figure, we infer that the dynamics exhibited by the defects of the traveling waves has a turbulentlike nature [24]. Further increasing the translational coupling parameter δ, the spatiotemporal intermittency is replaced by the permanent or almost uniform emergence of defects [see Fig. 2(d)]. Namely, the appearance of defects is not intermittent. From the behavior of the envelope and its respective power spectrum, we conclude that this type of spatiotemporal dynamics corresponds to defect turbulence [23]. The power spectrum is characterized by maintaining a

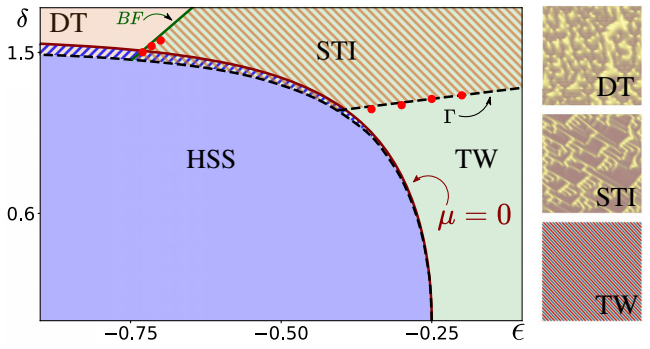

FIG. 3. Phase diagram of the Swift-Hohenberg model with translational coupling Eq. (1) with $\nu = 1.0$. HSS, TW, STI, and DT account for the homogeneous steady state $u = 0$, traveling wave with uniform envelope, spatiotemporal intermittency, and, defect turbulence, respectively. The solid (red) curve, $\mu = 0$, accounts for the convective instability. The solid curve BF describes the Benjamin-Fair instability. The dashed line Γ accounts for the transition between spatiotemporal intermittency to traveling waves. Red dots are the transition lines obtained by direct numerical simulations. The insets show the respective dynamic behaviors observed.

power law for large wave number $S(k) \sim k^{-5}$. From the point of view of defect production, it is not possible to identify the transition between spatiotemporal intermittency and defects turbulence. An efficient way to determine this transition is characterizing the statistics of regular and irregular regions of spatiotemporal evolution [25,26]. From defect turbulence equilibrium, when one decreases δ the emergence of spatiotemporal intermittency is observed, which remains in a large area of the parameter space coexisting with the uniform traveling wave. Hence, spatiotemporal intermittency presents a hysteresis loop with the traveling wave of uniform amplitude. Figure 3 shows the numerical phase diagram of the Swift-Hohenberg model with translational coupling Eq. (1).

To shed light on the origin of the previous dynamical behaviors, we will perform a weakly nonlinear analysis. Close to the transition between the homogeneous state and the traveling waves, *convective instability* induced by the nonlocal term [27,28], we can introduce the envelope ansatz

$$u(x,t) = aAe^{i(k_c y - \omega_c t)} + a\bar{A}e^{-i(k_c y - \omega_c t)} + W(A,\bar{A}), \quad (2)$$

in Eq. (1), where A is the complex amplitude of the critical wave, k_c is the critical wave number that satisfies the relation $k_c^4 = \epsilon\cos(k_c\delta) + \nu k_c^2$, $\omega_c = \epsilon\sin(k_c\delta)$ is the wave frequency, $\mu = \Delta\epsilon\cos(k_c\delta) - \epsilon k_c\Delta\delta\sin(k_c\delta)$ is the bifurcation parameter that characterizes the convective instability, $a = 1/\sqrt{3\cos(k_c\delta)}$ is a normalization constant, and $W(A,\bar{A})$ accounts for nonlinear corrections in amplitude A. Linearizing in W and imposing a solvability condition, the amplitude satisfies the convective and complex Ginzburg-Landau equation [29]

$$\partial_t A = \mu A - (1 + i\beta)|A|^2 A + (1 + i\alpha)\partial_z^2 A + v\partial_z A, \quad (3)$$

where the dimensionless spatial coordinate $z \equiv x/z_0$ with $z_0 = \sqrt{6k_c^2 - \nu + \varepsilon\delta^2 \cos(k_c\delta)/2}$, diffraction $\alpha \equiv \varepsilon\delta^2 \sin(k_c\delta)/2z_0^2$, nonlinear frequency response $\beta \equiv \tan(k_c\delta)$, and advective speed $v = \varepsilon\delta \cos(k_c\delta)/z_0$.

In the limit of local dynamic, $\delta = 0$, one recovers the Ginzburg-Landau equation with real coefficients ($\alpha = \beta = v = \omega = 0$), which describes the emergence of patterns [3]. In the case of periodic boundary conditions by considering the comobile coordinate system, the advective term in Eq. (3) can be eliminated. However, for other boundary conditions, this advective term is relevant to explain the transition from convective and absolute instability [27] and pinning-depinning of patterns [30]. The bifurcation parameter $\mu = 0$ accounts for the convective instability of the homogeneous state (see Fig. 3). This instability gives rise to a family of traveling waves of the form $A_p(y,t) = \sqrt{\mu - p^2}e^{i[py+(v-\beta(\mu-p^2)-\alpha p^2)t]}$. Stability analysis of this traveling wave for $p = 0$, allows obtaining the Benjamin-Fair (BF) critical curve, $1 + \alpha\beta = 0$ [29]. Figure 3 shows the BF curve in the parameter space $\{\epsilon, \delta\}$. It is expected to find phase turbulence for small β and significant α [23]. However, this is not possible to observe for the parameters generated from the $\{\epsilon, \delta\}$ space. The only phenomenon observed from the Ginzburg-Landau equation is the transition from waves to defect turbulence, which is expected for small α and large β [23]. It is also well known that this instability is of a subcritical nature; that is, coexistence is observed between the defects turbulence and traveling waves. By decreasing the parameter of instability, the defects' turbulence is replaced by spatiotemporal intermittency, which coexists with the traveling waves. Note that this dynamical behavior is consistent with the phenomena observed in the spatiotemporal intermittency region in Fig. 3. The transition between spatiotemporal intermittency to traveling waves was characterized numerically [23]. Using this numerical characterization, we have interpolate this transition curve, indexed by Γ, in the phase space represented in Fig. 3. In brief, the Ginzburg-Landau equation allows us to reveal the origin of all the intricate dynamics exhibited by the prototype pattern formation model with the translational coupling Eq. (1).

To compare the entire previous scenario with experimental observations onto the liquid crystal light valve with optical translational feedback, we must first consider more realistic boundary conditions than periodic ones and adequate domain of simulation. We have conducted numerical simulations of model Eq. (1), where a few numbers of wavelength is allowed. Note that experimentally, we observe about 20 wavelengths. Furthermore, we have considered Dirichlet boundary conditions $u(y = 0, t) = u(y = L, t) = 0$.

Experimentally and numerically, the parameters are in the region where pattern formation is observed. When a small translational length is included, we observe a static pattern due to pinning, induced by the boundary conditions [30] (see top panels in Fig. 4). When δ is increased, the pattern become propagative, but as a consequence of the boundary conditions, systematically appear and disappear dislocations in the spatiotemporal diagrams [cf. Figs. 4(b) and 4(e)]. Further increasing the translational coupling length, patterns exhibit intermittent behaviors, characterized by having a power spectrum with power laws. Figure 4 summarizes the spatiotemporal evolution of the pattern observed in the model Eq. (1) and the liquid crystal valve

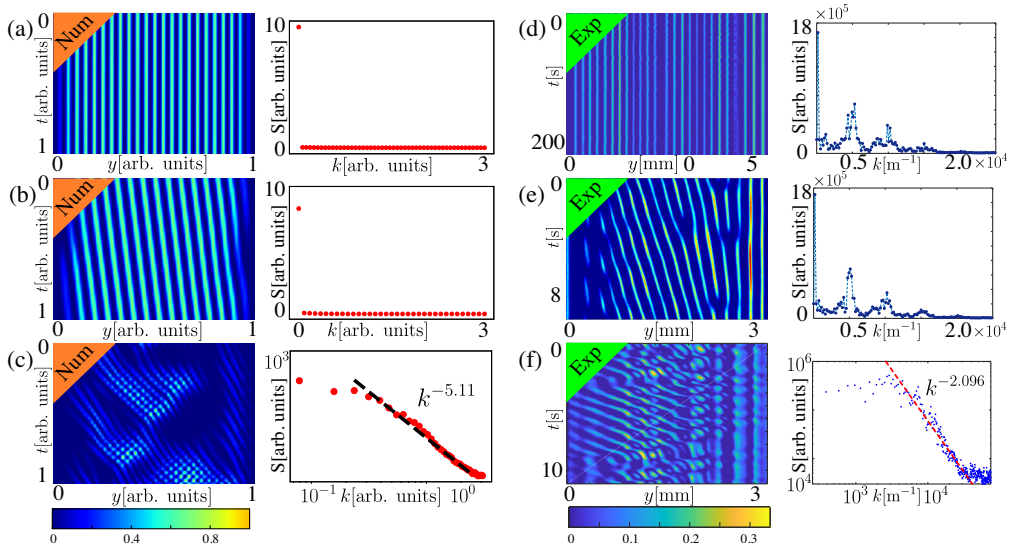

FIG. 4. Spatiotemporal evolution and the temporal average power spectra $S(k)$ of the envelope of the pattern observed in the model Eq. (1) by $\epsilon = -0.1$ and the liquid crystal valve with translational optical feedback. Left panels: numerical simulations with $\delta = 0.0$ (a), 0.2 (b), and 1.51(c). Right panels: experimental observations with $\delta = 0 \pm 5$ μm (d), $\delta = 25 \pm 5$ μm (e), and $\delta = 50 \pm 5$ μm (f).

with optical translated feedback. Hence, experimental observations and sequence of transitions have a qualitative agreement with theoretical findings. However, the critical exponents of the spatiotemporal intermittency are not the same. Theoretical characterization from a first principles model is in progress.

In conclusion, we have shown that systems under translational coupling exhibit transition to spatiotemporal intermittency and turbulence of defects. The translational coupling can be described as an asymmetric differential integral term. This type of coupling has been used to describe various systems in population dynamics, nonlinear optics, fluids, and ecology. Hence, the results presented are relevant in various physical contexts.

The authors thank F. del Campo for his discussions and primary numerical observations. We wish to acknowledge the economic support of Millennium Institute for Research in Optics and Fondecyt 1180903. G. G.-C. acknowledges the support of CONICYT-PFCHA Doctorado Nacional 2017211716.

[1] P. Glansdorff and I. Prigogine, *Thermodynamic Theory of Structures. Stability and Fluctuations* (Wiley, New York, 1971).
[2] G. Nicolis and I. Prigogine, *Self-Organization in Non-equilibrium Systems* (John Wiley & Sons, New York, 1977).
[3] L. M. Pismen, *Patterns and Interfaces in Dissipative Dynamics* (Springer, Berlin, 2006).
[4] M. Cross and H. Greenside, *Pattern Formation and Dynamics in Non-Equilibrium Systems* (Cambridge University, New York, 2009).
[5] A. C. Newell, T. Passot, and J. Lega, Annu. Rev. Fluid Mech. **25**, 399 (1993).
[6] R. B. Hoyle, *Pattern Formation: An Introduction to Methods* (Cambridge University Press, Cambridge, England, 2006).
[7] A. O. Leon, M. G. Clerc, and S. Coulibaly, Phys. Rev. E **89**, 022908 (2014).
[8] F. T. Arecchi, S. Boccaletti, and P. Ramazza, Phys. Rep. **318**, 1 (1999).
[9] P. L. Ramazza, S. Ducci, and F. T. Arecchi, Phys. Rev. Lett. **81**, 4128 (1998).
[10] G. Agez, P. Glorieux, M. Taki, and E. Louvergneaux, Phys. Rev. A **74**, 043814 (2006).
[11] F. del Campo, F. Haudin, R. G. Rojas, U. Bortolozzo, M. G. Clerc, and S. Residori, Phys. Rev. E **86**, 036201 (2012).
[12] F. Haudin, R. G. Rojas, U. Bortolozzo, M. G. Clerc, and S. Residori, Phys. Rev. Lett. **106**, 063901 (2011).
[13] J. D. Murray, *Mathematical Biology* (Springer, New York, 1990).
[14] E. Meron, *Nonlinear Physics of Ecosystems* (CRC Press, Boca Raton, 2015).
[15] M. G. Clerc, S. Coulibaly, and M. Tlidi, Phys. Rev. Research **2**, 013024 (2020).
[16] J. Swift and P. C. Hohenberg, Phys. Rev. A **15**, 319 (1977).
[17] J. H. P. Dawes, Historia mathematica **43**, 49 (2016).
[18] S. Residori, Phys. Rep. **416**, 201 (2005).
[19] M. G. Clerc, G. Gonzalez-Cortes, V. Odent, and M. Wilson, Opt. Express **24**, 15478 (2016).
[20] J. Swift and P. C. Hohenberg, Phys. Rev. A **15**, 319 (1977).
[21] J. Claerbout, *Fundamentals of Geophysical Data Processing* (McGraw-Hill, New York, 1976).
[22] M. G. Clerc, S. Coulibaly, F. del Campo, M. A. Garcia-Nustes, E. Louvergneaux, and M. Wilson, Phys. Rev. E **92**, 050902(R) (2015).
[23] H. Chate, Nonlinearity **7**, 185 (1994).
[24] U. Frisch, *Turbulence: The Legacy of AN Kolmogorov* (Cambridge University Press, Cambridge, England, 1995).
[25] S. Ciliberto and P. Bigazzi, Phys. Rev. Lett. **60**, 286 (1988).
[26] S. Coulibaly, M. Taki, A. Bendahmane, G. Millot, B. Kibler, and M. G. Clerc, Phys. Rev. X **9**, 011054 (2019).
[27] R. J. Briggs, *Electron-Stream Interaction with Plasmas* (MIT Press, Cambridge, MA, 1964).
[28] F. Papoff and R. Zambrini, Phys. Rev. Lett. **94**, 243903 (2005); Phys. Rev. E **73**, 016611 (2006); Eur. Phys. J. D **58**, 235 (2010).
[29] I. S. Aranson and L. Kramer, Rev. Mod. Phys. **74**, 99 (2002).
[30] M. G. Clerc, C. Fernandez-Oto, M. A. Garcia-Nustes, and E. Louvergneaux, Phys. Rev. Lett. **109**, 104101 (2012).